HELDA
HELSINGIN YLIOPISTO
HELSINGFORS UNIVERSITET
UNIVERSITY OF HELSINKI

UNIVERSITY OF HELSINKI

https://helda.helsinki.fi

Combining Experimental and DFT Investigation of the Mechanism Involved in Thermal Etching of Titanium Nitride Using Alternate Exposures of NbF5 and CCl4, or CCl4 Only

Sharma, Varun

2021-11

Sharma , V , Natarajan , S K , Elliott , S D , Blomberg , T , Haukka , S , Givens , M E , Tuominen , M & Ritala , M 2021 , ' Combining Experimental and DFT Investigation of the Mechanism Involved in Thermal Etching of Titanium Nitride Using Alternate Exposures of NbF5 and CCl4, or CCl4 Only ' , Advanced Materials Interfaces , vol. 8 , no. 22 , 2101085 . https://doi.org/10.1002/ac

http://hdl.handle.net/10138/350070
https://doi.org/10.1002/admi.202101085

unspecified
acceptedVersion

Downloaded from Helda, University of Helsinki institutional repository.

This is an electronic reprint of the original article.

This reprint may differ from the original in pagination and typographic detail.

Please cite the original version.

Combining Experimental and DFT Investigation of the Mechanism Involved in Thermal Etching of Titanium Nitride Using Alternate Exposures of NbF_5 and CCl_4, or CCl_4 only

Varun Sharma,[*,†,‡] Suresh Kondati Natarajan,[¶] Simon D. Elliott,[§] Tom Blomberg,[‖] Suvi Haukka,[†] Michael E. Givens,[†] Marko Tuominen,[†] and Mikko Ritala[*,‡]

†ASM Microchemistry Oy, Pietari Kalmin katu 3 F2, Helsinki, Uusimaa 00560, Finland

‡Department of Chemistry, University of Helsinki, Helsinki, Uusimaa 00014, Finland

¶Department of Electrical Engineering and Automation, Aalto University, Espoo 02156, Finland

§Schrödinger, 120 West 45th Street, New York, New York 10036-4041, USA

‖Department of Chemistry and Materials Science, Aalto University, Espoo, Uusimaa 02150, Finland

E-mail: varun.sharma@asm.com,varun.sharma@helsinki.fi; mikko.ritala@helsinki.fi

Abstract

Thermally activated chemical vapor-phase etching (CVE) of titanium nitride (TiN) was studied by utilizing either alternate exposures of niobium pentafluoride (NbF_5) and carbon tetrachloride (CCl_4) or by using CCl_4 alone. Nitrogen (N_2) gas purge steps were carried out

in between every reactant exposure. Titanium nitride is etched in a non self-limiting way by NbF_5 - CCl_4 based binary chemistry or by CCl_4 at temperatures between 370 and 460°C. Spectroscopic ellipsometry and a weight balance were used to calculate the etch per cycle. For the binary chemistry, an etch per cycle of about 0.8 Å was obtained for 0.5 s and 3 s long exposures of NbF_5 and CCl_4, respectively at 460°C. On the contrary, under the same conditions, the etch process with CCl_4 alone gave an etch per cycle of about 0.5 Å. In the CCl_4-only etch process, the thickness of TiN films removed at 460°C varied linearly with the number of etch cycles. Furthermore, CCl_4 alone is able to etch TiN selectively over other materials such as Al_2O_3, SiO_2 and Si_3N_4. X-ray photoelectron spectroscopy (XPS) and bright field transmission electron microscopy (BF-TEM) were used for studying the post-etch surfaces. To understand possible reaction products and energetics, first-principles calculations were carried out with density functional theory. From thermochemical analysis of possible reaction models, it was found that NbF_5 alone can not etch TiN while CCl_4 alone can etch it at high temperatures. The predicted by-products of the reaction between the CCl_4 gas molecules and TiN surface are $TiCl_3$ and ClCN. Similarly, TiF_4, $NbFCl_3$ and ClCN are predicted to be the likely products when TiN is exposed to both NbF_5 and CCl_4. A more favourable etch reaction is predicted when TiN is exposed to both NbF_5 and CCl_4 (Gibbs free energy, ΔG = -2.1 eV at 500 K) as compared to exposure to CCl_4 only (ΔG = -1.5 eV at 500 K) process. This indicates that an enhanced etch rate is possible when TiN is exposed alternately to both NbF_5 and CCl_4, which is in close agreement with the experimental results.

Introduction

With the continuous scaling of device dimensions in integrated circuits, more complex 3D device architectures are constantly being developed.[1,2] In order to keep developing such non-line-of-sight features, processing techniques that provide conformal as well as precise control of thickness at the atomic scale have become indispensable.[3–5] Deposition and etching are two of the most widely employed techniques in the fabrication of today's nanoelectronic devices. Semiconductor tool manufacturers have stretched their limits to gain atomic precision when depositing and etching

various materials.[3–7] Atomic layer deposition is a well established chemical gas phase deposition technique with hundreds of reported processes.[8,9] On the other hand, reports on plasma-free chemical-based etch processes are limited and especially so for the recently developed thermal atomic layer etching (ALE).[10,11] Thermal ALE is a technique that uses sequential self-limiting surface-gas reactions in order to etch material from the surface.[12] The self-limiting surface reactions may provide important advantages, such as isotropic etching,[11,12] thickness control in the atomic regime and possibly improved etch selectivity. Therefore, thermal ALE a is promising technique for fabricating non-line-of-sight features in 3D nanoscale devices.

Titanium nitride (TiN) is a crucial material for the semiconductor industry due to its CMOS compatibility and has found use in applications such as tunable work-function metal gate[13] in fin-field-effect-transistor (FinFET) and gate-all-around (GAA) nanowire metal-oxide-semiconductor-field-effect-transistor (NWFET),[14] gate electrode in metal–insulator–semiconductor field effect transistor (MISFET),[15] diffusion barrier,[16] metal hard mask,[17] anti-reflective coating,[18] extreme ultra-violet (EUV) patterning,[19] sub-bandgap[20] and Schottky photodetector,[21] and in plasmonics.[22,23]

So far, most of the TiN etch processes utilize either solutions[24–26] or plasma chemistries,[27–30] and a very few purely vapor etch processes have been reported.[31,32] Lee et. al.[31] proposed a conversion-etch mechanism for TiN. First, the surface of the TiN films was oxidized to TiO_2 by ozone (O_3) and then TiO_2 was etched by HF vapor in the form of volatile TiF_4 and H_2O species. Ozone is a strong oxidant[31] and is capable of oxidizing also other materials in the vicinity on the integrated circuit chips. HF is toxic and its use may result in the dreaded fluorine contamination that not only affects the performance of CMOS devices but also poses compatibility issues with storage as well as semiconductor processing equipment. Thus, new thermal processes with other etchants for TiN would be beneficial in fabricating complex devices.

We report novel chemical etching processes for titanium nitride. Two types of etching processes were studied: first, a two-step gas-surface reaction based on sequential exposures of NbF_5 - CCl_4 reactants, and secondly a spontaneous etching by CCl_4 alone which can be defined as gas-phase

pulsed etching (GPPE).[32] N_2 purge steps were introduced in between reactant pulses to avoid any reactant overlap, and to purge the etch system from excess reactant molecules as well as reaction products.

First principles calculations using density functional theory (DFT) are employed to study the thermochemistry of the reactions involved in the etch process. First principles calculations provide an effective approach for evaluating the free energies of the etch reactions. This is particularly important in this study as many exotic chemical species may be involved in the reaction for which experimental thermodynamic data are not available in the literature. We also use DFT to predict probable etch products from the product pressures evaluated at thermodynamic equilibrium.

Experiment

Substrates and process gases

P-doped silicon wafers of 200 mm diameter were chosen as substrates. The target films subjected to etching were SiO_2, Si_3N_4, Al_2O_3 and TiN. The SiO_2 was either thermally grown silicon oxide of about 22 nm thick or 15 nm SiO_2 grown by the plasma-enhanced atomic layer deposition (PEALD) technique.[33] A 20 nm thick LPCVD nitride (Si_3N_4) was used. Al_2O_3 of about 20 nm was deposited at 300°C by the trimethylaluminum (TMA) and water (H_2O) ALD process.[34] TiN was deposited on 22 nm thermal oxide at 400°C by thermal ALD process utilizing $TiCl_4$ and NH_3.[35] The TiN films used in these etch experiments were from 10 to 50 nm in thickness.

NbF_5 (98 %, CAS Number 7783-68-8) and anhydrous CCl_4 (CAS Number 56-23-5) were purchased from Sigma Aldrich, Inc. (Germany). The NbF_5 vessel was kept at 45-50 °C. The CCl_4 vessel was kept at room temperature and the vapors were drawn into the chamber. The CCl_4 dose was controlled by a needle valve and the NbF_5 outlet line did not have the needle valve installed. Nitrogen of 5.0 purity was used as a carrier gas, and was further purified by a purifier to $\geq$ 6.0 level.

Experimental setup and methodology

The etch experiments were performed in a Pulsar® 2000 (P2000) reaction chamber, manufactured by ASM. The etch temperature was varied from 370 to 460°C under isothermal conditions. Due to the hardware limitation of this particular P2000 module, the 460°C was the maximum obtainable temperature and therefore the choice of the range. This temperature range may require highly thermally stable reactants such as CCl_4[36] and NbF_5.[37,38] More details of a setup and methodology can be found in an earlier reports.[32,39]

The etch rate per cycle (EPC) was calculated from the removed thickness values. Before and after etching, the thickness values were determined by spectroscopic ellipsometry (SE) and weight measurements as described earlier.[32] In order to verify the etch process, in-situ grown TiN films were also subjected to etching. No significant differences in EPC were found between air-oxidized and in-situ grown TiN films. In some cases, an X-ray reflectometer was also used to confirm the thickness and extract density values of TiN films. For simplicity, EPC values reported here are extracted from the weight measurements except in Fig. 4, where SE thickness values are reported.

Characterization techniques and equipment

An SAG 204 balance from Mettler Toledo with a resolution of about 0.1 mg was used for the weight measurements. The EPC and removed thickness values were extracted by using simple mass-density-volume relationship, as described in previous report.[32]

For thickness, optical constants and density measurements the SE 800 (from SENTECH) ellipsometer and X'pert PRO XRR (from Malvern Panalytical Ltd.) were used.

The surface composition as well as depth profiles were determined with the help of X-ray photoelectron spectroscopy (XPS). The XPS used here was a K-Alpha+ from Thermo Scientific™. The aluminum Kα (1486.6 eV / 15 kV) X-ray source was used with a spot size of about 400 µm. In the XPS depth profile measurements, the argon ion energy was set to 1000 eV. For the survey scan, a total of 10 scans were performed with a pass energy of 200 eV, and an increment of 0.5 eV.

The transmission electron microscopy was executed by Evans Analytical Group (EAG), Cal-

ifornia. For the imaging the FEI Tecnai TF-20 FEG/TEM operated at 200kV was used in the bright-field TEM mode. For the sample preparation, an in-situ focused ion beam (FIB) lift-out technique on an FEI Dual Beam FIB/SEM was used. Prior to the ion milling, the samples were carbon coated followed by sputtering iridium on top. The thickness of the TEM lamella was about 100 nm.

Theory and computational setup

The Vienna Ab initio Simulation Package (VASP v5.3)[40,41] was used for the quantum chemical calculations reported in this manuscript. We have used spin-polarized density functional theory (DFT) to describe the electronic structure of the system under study. The exchange-correlation interactions are approximated by the Perdew-Burke-Ernzerhof (PBE)[42] generalized gradient corrected density functional. The valence electrons are expanded in a plane wave basis set with a 400 eV cutoff, whereas the core electrons are treated by projector augmented wave (PAW) potentials.[43] The PAW potentials have 13 valence electrons for Nb, 4 for Ti, 5 for N and 7 each for F and Cl. The geometries are relaxed within 1 meV of energy and within 0.02 eV/Å of magnitude of each force component.

The cubic phase of TiN (space group $Fm\bar{3}m$) is chosen for the DFT study. The bulk unit cell consists of 4 TiN units and its shape and volume are simultaneously relaxed with a higher energy cutoff of 550 eV. A Monkhorst-Pack k-point mesh of $6\times6\times6$ is used to sample the first Brillouin zone. The minimum energies of the isolated molecules are computed by optimizing their geometries within a non-cubic box of dimensions 15 Å$\times$ 16 Å$\times$ 15.5 Å. The computation setup for the surface reaction are given in section S0 of the SI.

For the reaction free energy computation, the free energy of a system at a given temperature T is given by

$$G = E + H - TS, \tag{1}$$

in which E is the electronic energy of the system, H is the enthalpy and S is the entropy. Enthalpy

and entropy of gas phase species are obtained from the 'freeh' tool in the TURBOMOLE suite.[44] The enthalpy and entropy of bulk systems are obtained with the Phonopy code,[45] which uses the force constants obtained from a density functional perturbation theory calculation in VASP with an energy threshold of $1.0e^{-8}$ eV for the self consistent field evaluation of the electronic energy. The reaction free energy is then computed as

$$\Delta G = \Delta E + \Delta H - T\Delta S + RT\ln\left(\prod \mathrm{P}^{\mathrm{np}}_{\mathrm{products}} / \prod \mathrm{P}^{\mathrm{nr}}_{\mathrm{reactants}}\right), \quad (2)$$

in which the Δ symbol signifies difference between the product and reactant state contributions. The 'np' and 'nr' are the number of gas phase molecules in the product state and reactant state, respectively. *P* is pressure and *R* is the gas constant. We can also calculate product pressure P_p at an user defined temperature T that will bring ΔG=0. If at some temperature T ΔG without the RTln(Q) term is positive, then P_p value must be lowered to bring the reaction to equilibrium and *vice-versa*. A very low value of P_p indicates that the corresponding reaction by-products are less likely at that temperature and *vice-versa*. Please note that this analysis cannot be used to obtain the product pressure value in equation 2.

Results and Discussion

Thermochemistry: Free Energies of Proposed Reactions

Let us start by discussing the thermochemistry of the overall etch cycle and the individual reactant pulses using DFT data. In Table 1 we show the reaction free energies for a number of reactions postulated for the overall etch cycle considering a reactant pressure of 2.5 Torr and a product pressure of 0.01 Torr. Please note that the product pressure cannot be controlled in an etch reactor and it is typically much lower than the reactant pressure, so we choose a value of 0.01 Torr for our calculations.

In reactions R1-R5, we consider a unit of bulk TiN reacting simultaneously with 1 NbF_5 and

1 CCl_4 molecules to form different gas phase products. It is to be noted that Nb can take different oxidation states and thus there are very many possible combinations of volatile products. Since it is not practical to consider all of them, we have computed a small set of representative product combinations.

Table 1: A list of reactions and computed thermochemistry representing the overall etch process in which 1 solid TiN bulk unit is converted into gas phase products on reacting with 1 NbF_5 and 1 CCl_4 molecules. R2, R4 and R5 (shown in bold font) are redox reactions. All species other than TiN are in gas phase. P_p at ΔG=0 is the product pressure at 740 K that will bring the reaction to equilibrium at a constant reactant pressure of 2.5 Torr. A low P_p value indicates the reaction products are unlikely and vice-versa.

Reactions	ΔG [eV]		P_p [Torr]
	640 K	740 K	at ΔG=0; T=740 K
R1: $1TiN + 1NbF_5 + 1CCl_4 \longrightarrow 1TiCl_3 + 1NbNFCl + 1CF_4$	2.8	2.5	7.3E-14
R2: $1TiN + 1NbF_5 + 1CCl_4 \longrightarrow 1TiCl_4 + 1NbNF + 1CF_4$	3.3	2.9	1.5E-15
R3: $1TiN + 1NbF_5 + 1CCl_4 \longrightarrow 1TiCl_3 + 1NbClF_4 + 1CNF$	-1.2	-1.6	3.8E+00
R4: $1TiN + 1NbF_5 + 1CCl_4 \longrightarrow 1TiCl_4 + 1NbF_4 + 1CNF$	-0.8	-1.2	1.4E-01
R5: $1TiN + 1NbF_5 + 1CCl_4 \longrightarrow 1TiF_4 + 1NbFCl_3 + 1ClCN$	-2.7	-3.1	3.8E+05

Table 2: Potential reactions of individual reagent pulses with bulk TiN in the etch process, assessed via thermochemistry computed with DFT. R6 - R8 represent the fluorination pulse and R9 represents the chlorination pulse. P_p at ΔG=0 is the product pressure at 740 K that will bring the reaction to equilibrium at a constant reactant pressure of 2.5 Torr. A low P_p value indicates the reaction products are unlikely and vice-versa.

	Reactions	ΔG [eV]		P_p [Torr]
		640 K	740 K	at ΔG=0; T=740 K
R6:	$1TiN + 1NbF_5 \longrightarrow 1TiNF + 1NbF_4$	6.1	5.7	7.3E-24
R7:	$1TiN + 1NbF_5 \longrightarrow 1TiF_3 + 1NbNF_2$	3.5	3.1	4.2E-15
R8:	$1TiN + 1NbF_5 \longrightarrow 1TiF_4 + 1NbNF$	3.9	3.5	2.5E-16
R9:	$1TiN + 1CCl_4 \longrightarrow 1TiCl_3 + 1ClCN$	-2	-2.4	1.8E+04

The reactions R2, R4 and R5 (with labels in bold font in Table 1) are redox reactions in which the Ti atoms are oxidized and Nb atoms are reduced. The production of gaseous products is often entropically favored and therefore the reaction free energies decrease as the temperature is increased to 740 K (467°C), with R5 being the most favourable at ΔG=-3.1 eV. R3 and R4 become favourable at 740 K although not as favourable as R5. At 640 K (367°C), the favourable reactions

are R3, R4, R5 and R9. R1 and R2 are more unlikely compared to R3 and R4 not because of the Ti compound but because of the Nb and C compounds. From the reaction energies, Nb-N compounds are found to be less favorable in gas phase when compared to C-N compounds. For a similar reason, R3 and R4 are more favorable than R1 and R2, respectively, although both reactions in each set form the same Ti compound. R5 is the most favorable, because it results in a C-N compound and TiF_4, which is a well known volatile and stable gas molecule. The TiF_3 as a by-product was not considered due to its high boiling point of 1400°C[31] and non-volatility,[31,46] especially within the experimented temperature range i.e. 370-460°C.

Even at 740 K, the calculations show that reactions R1 and R2 are not favourable as the change in Gibbs free energy is +2.5 and +2.9 eV, respectively. The product pressure evaluated at $\Delta G = 0$ and 740 K gives an indication of the likelihood of the formation of the considered reaction products. This value is very small for R1 and R2 suggesting that NbNF/Cl and CF_4 are not very probable products. On the other hand, a high product pressure at $\Delta G = 0$ and 740 K is registered for reaction R5 indicating an increased likelihood in the formation of the volatile products TiF_4, $NbFCl_3$ and ClCN, hence the etching.

The reactions where N_2 is an etch product were also considered, and are as follows: $2TiN(s) + 6NbF_5(g) + 6CCl_4(g) \longrightarrow 6NbFCl_3(g) + N_2(g) + 2TiCl_3(g) + 6CF_4(g)$, and $2TiN(s) + 8NbF_5(g) + 8CCl_4(g) \longrightarrow 8NbFCl_3(g) + N_2(g) + 2TiCl_4(g) + 8CF_4(g)$. Both the reactions are highly endothermic and unfavorable even at 500 K with reaction energies of 9.5 eV and 8.5 eV, respectively.

In Table 2, we consider representative etch reactions (R6 - R9) in the individual pulses when either NbF_5 or CCl_4 is used as reactant. The fluorination pulse is presented as reactions R6 - R8, in which NbF_5 may interact with TiN and form gas phase TiF_x and $NbNF_y$ species. The reaction free energies are very high (+3.1 to +5.7 eV at 740 K). The product pressure at $\Delta G = 0$ and 740 K is correspondingly very small. This indicates that etch reactions are not possible when pulsing only NbF_5 mainly due to the unfavorable Nb-N compounds. The adsorption mechanism of NbF_5 on the TiN surface has been computed and is described in section S1 of the SI. We find that NbF_5 dissociates on the TiN(211) surface spontaneously at 400 K and results in the formation of strong

surface bound Ti-F and Nb-N bonds (see section S1 of the SI). Thermodynamically, the Ti-F bonds on TiN surface are more stable and favourable when compared to Ti-Cl bonds (see section S3 of the SI). The formation of any gas phase byproducts was not observed from the DFT simulations of the fluorination pulse.

Reaction R9 shows the TiN etch reaction by CCl_4 and a spontaneous etching at 640 and 740 K, as evidenced by the negative free energy change, is observed. The preferred products are $TiCl_3$ and ClCN. Expressed in another way, the product pressure at $\Delta G = 0$ and 740 K is very large. From simulations, we also found that CCl_4 molecule dissociated spontaneously on TiN(211) surface (see section S2 of the SI).

Thus, the first principles thermochemistry suggests that the NbF_5 pulse could not etch (TiN) by itself, while the CCl_4 pulse alone could etch (TiN) spontaneously, however subject to kinetic barriers. Comparing R5 and R9, the combination of (NbF5) and (CCl4) pulses at 740 K is predicted to give more effective etching of TiN than etching by CCl_4 alone. The C compound in the two reactions is the same ClCN and the Ti compounds $TiCl_3$ and TiF_4 have very similar thermochemistry as well. However, $NbFCl_3$ offers lower zero point energy and higher entropy than NbF_5 which allowed R5 to have a lower reaction free energy than R9.

From simulations, a CCl_4 is found to dissociate spontaneously at a surface bound fluorine free Nb site - which is the precursor for the formation of NbF_xCl_y species in R9. Please refer to section S2 of the SI for more information on the explicit reaction mechanisms that have been computed with DFT for this etch process. This enhanced etching phenomenon with sequential pulses of NbF_5 and CCl_4 is experimentally verified and observed in figures 2 and 3.

Experimental etching characteristics

TiN films were etched by two types of etch processes: (1) a binary process that involves alternating exposures of NbF_5 and CCl_4 reactants in a cyclic manner and (2) a pulsing CCl_4 alone in a chemical vapor etching (CVE) or GPPE process. One cycle of pulsed CVE of TiN films consists of a CCl_4 exposure followed by an inert gas (N_2) purge. The N_2 purges were introduced to ensure the

products and excess precursor molecules were removed properly from the etch system.

In this context, an etch system is an aggregate term used to describe all the components such as gas lines, valves and the reaction chamber and its parts. The concept and feasibility studies performed under this section demonstrate TiN etching in the atomic regime. The CCl_4 based CVE process provides selectivity over Al_2O_3, SiO_2, and Si_3N_4. However, the NbF_5 - CCl_4 based etch process is able to etch Al_2O_3 and provides selectivity over SiO_2 and Si_3N_4.

Figure 1 shows a change in the TiN EPC with varying NbF_5 pulse time for the NbF_5 - CCl_4 etch process at 460°C and 1 s long CCl_4 pulse time. The etch temperature of 460°C was chosen because it was limited by the hardware. The figure reveals that when no NbF_5 is used, an EPC of 0.3 Å is obtained which indicates that CCl_4 alone is capable of etching TiN films as will be discussed later. This is consistent with the favorable thermochemistry that is predicted with DFT. The EPC increases from 0.3 to about 0.6 Å when the NbF_5 pulse time is varied from 0 to 1 s. At 3 s NbF_5 pulse time an EPC of about 0.8 Å is measured. There is no clear saturation of EPC with the NbF_5 pulse time, but a marginal slowing of an EPC is observed. We speculate that this non-saturated behaviour can be attributed to various factors such as partially self-limiting nature of the surface reaction, insufficient purge time, low volatility or otherwise slow removal of the products from the TiN surface and presence of finite vapors of CCl_4 in the etch system. This soft-saturation of the EPC with NbF_5 pulse time can also be assigned to a slow diffusion of F species through grain boundaries to form a converted TiN surface and form fluorinated TiN surface.

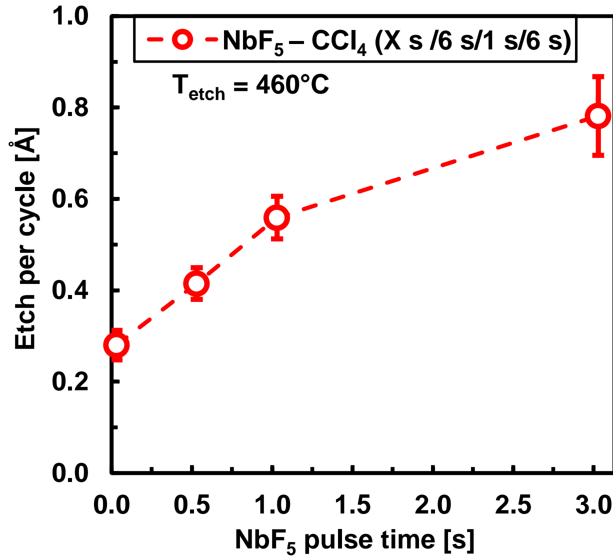

Figure 1: Etch per cycle for TiN films vs NbF_5 pulse time at 460°C. The duration of N_2 purges and CCl_4 pulses were fixed at 6 s and 1 s, respectively.

In Fig. 2 EPCs for two etch processes are plotted against CCl_4 pulse time at an etch temperature of 460°C. From the graph, it is worth noticing that the EPC for the NbF_5 - CCl_4 etch process is higher than that for the CCl_4 only CVE process. This holds true for a given set of process parameters such as gas flows, partial pressure of both the precursors, the pulse and purge times up to 3 s and 6 s, respectively, and total pressure of the reaction chamber.

The earlier presented first principles simulations also predicted a more favourable etch reaction for the NbF_5 - CCl_4 process than for CCl_4 only. For both etch processes, the EPC tends to increase with the CCl_4 pulse time.

Fig. 2 shows that no etching was observed when 0.5 s of NbF_5 and no CCl_4 was used, for total 300 cycles. No change in the TiN thickness was observed even after 300 cycles of 1 s NbF_5 pulse. At temperatures below 460°C, NbF_5 alone was not able to etch TiN by itself. This is consistent with the first principles simulations. The TiN thickness values before and after NbF_5 exposure were confirmed by XRR measurements.

For both etch processes, no clear saturation of EPC is observed. The EPC continues to increase linearly with CCl_4 pulse time from 0.5-3.0 s, with no sign of saturation. At 3 s long CCl_4 pulse time, EPC values of about 0.8 Å and 0.5 Å are observed for the NbF_5 - CCl_4 and CCl_4 only CVE

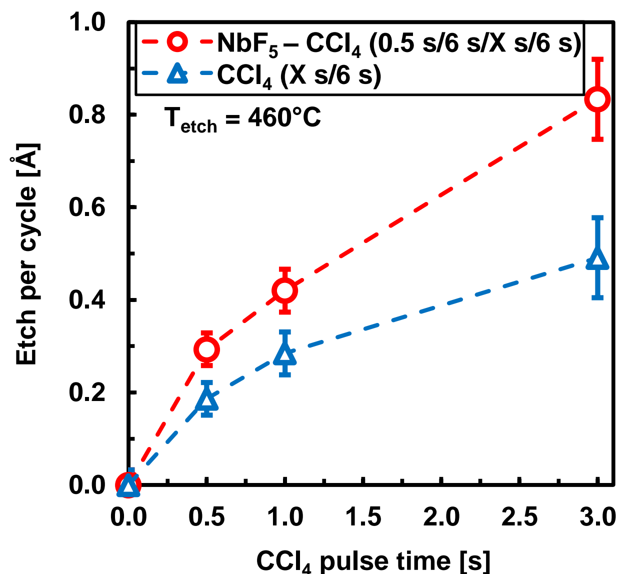

Figure 2: Etch per cycle of TiN films with varying CCl_4 pulse time at 460°C. 6 s long N_2 purges were used. The figure compares the EPC for the binary process (red) to the CVE process (blue).

processes, respectively. NbF_5 enhances the etch rate of TiN and this could be due to an enhanced reactivity of the CCl_4 with fluorinated TiN surface or the formation of more volatile species such as $TiCl_4$ (R5 in Table 1) instead of $TiCl_3$,[47] TiOCl or TiF_3. The $TiCl_3$ at 427 °C, has a sufficiently high vapor pressure of 37 mTorr.[48] On the contrary, TiF_3 has a very high boiling point of 1400°C[31] and is non-volatile.[31,46] The vapor pressures of $TiCl_4$ and TiF_4 at 90 °C are 190 Torr[49] and 18 mTorr,[50] respectively.

Another possible reason for the faster etching could be fluorine species diffusing through the TiN grain boundaries and therefore the etching may proceed three dimensionally rather than being limited to the surface. Later in FIG. 7 , the XPS depth profile analysis did show some fluorine penetration into the remaining TiN film, after exposing it to the NbF_5 - CCl_4 CVE process.

The simulation results provided in the SI (see S2 in the SI) reveal that the Nb sites are important for CCl_4 to react with when the rest of the surface is covered with F. It is found that the a favourable binding between the Cl atoms and Nb atom is possible (more details in the S2 of SI) even when the Nb atom is weakly bound to 2 F atoms. However, a strong dissociative adsorption of CCl_4 (-3.2 eV) is possible when the Nb atom is free of Nb-F bonds (see Figure S5 b) in the SI). Based on the computational results, we propose that the ALE of TiN proceeds by self-limiting

reaction of NbF_5 molecules with TiN surface in the first pulse (see S1 of the SI) followed by the dissociative adsorption of CCl_4 catalysed by the Nb sites in the second pulse leading to the etch of TiN. Additionally, from the 2 it can be seen that the NbF_5 alone did not etch TiN and is predicted by the computational results.

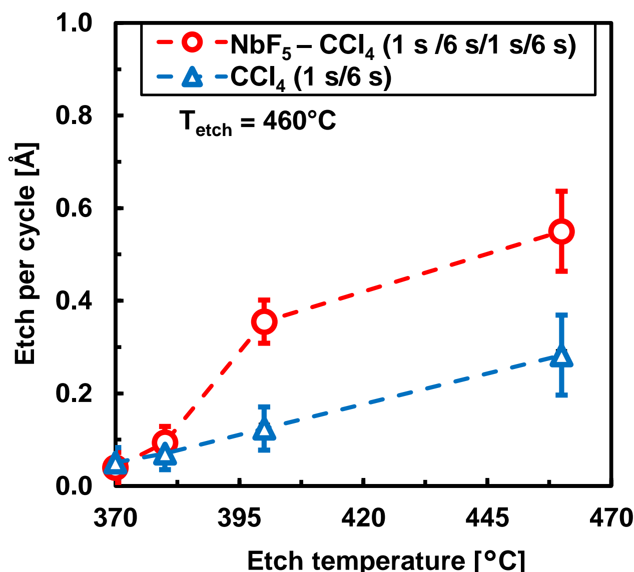

Figure 3: Effect of etch temperature on etch per cycle for the binary process (blue curve) as well as CCl_4 alone (blue curve) process. Both the precursor pulses and the purge times were fixed to 1 s and 6 s, respectively.

In figure 3, the effect of etch temperature on etch per cycle is captured for the both etch processes. The NbF_5 and CCl_4 pulse times were set to 1 s with 6 s long N_2 purges. For the data points in this graph, a total of 200, 200, 300 and 400 etch cycles were performed at etch temperatures of 370, 380, 400 and 460°C, respectively. For the NbF_5 - CCl_4 etch process, a low EPC of 0.03 Å/cycle at 370°C is obtained and the EPC increases almost linearly to about 0.4 Å/cycle at 400°C. At 460°C, a higher etch rate of 0.55 Å/cycle is noted. In contrast, the CCl_4 only etch process shows an etch rate of 0.07 Å/cycle at 370°C and linearly increases to about 0.3 Å/cycle at 460°C. Both the etch processes were unable to etch TiN significantly at temperatures below 370°C, even after total 1000 etch cycles. This is in disagreement with DFT thermochemistry predictions, which shows possible etching at 500 K (227° C) and the reason for this can be due to higher activation barrier.

Etch selectivity

Etch selectivity of TiN against different materials such as Al_2O_3, SiO_2 and Si_3N_4 was also studied for the reported etch processes. Figure 4 investigates the ability of the CCl_4 alone CVE process to etch TiN selectively over Al_2O_3, SiO_2 and Si_3N_4 at 460°C. The figure plots the etched thickness with the total number of etch cycles, where each cycle consisted of 1 s long CCl_4 pulse followed by 6 s long N_2 purge. EPC of 0.3 Å/cycle is deduced from a linear fit. After 500 etch cycles, about 13 nm TiN film is removed. No change in thickness is observed for Al_2O_3, SiO_2 and Si_3N_4 even after exposing them to 1000 cycles of 1 s long CCl_4 pulses. Moreover, at temperatures below 460°C, CCl_4 is unable to etch Al_2O_3, SiO_2 and Si_3N_4 either and therefore the selective etching of TiN is possible within temperature window of 370-460°C.

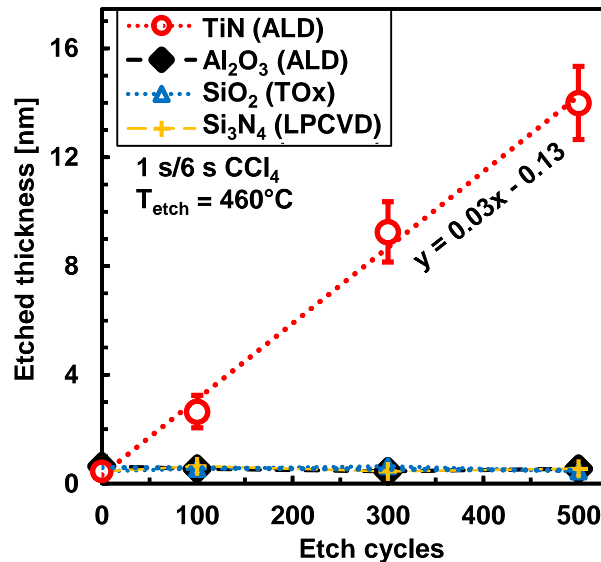

Figure 4: A change in the thickness values with total number of etch cycles at 460°C for TiN, SiO_2, Al_2O_3 and Si_3N_4 films. A TiN is selectively etched away by CCl_4 alone over other materials.

Post-etch analysis

After removing all 25 nm TiN film from the SiO_2 substrate, an ex situ XPS spectra of the post-etch surface was measured and is shown in figure 5. The main constituents of the remaining surface were 32.7 at. % Si, 60.9 at. % O, 5.1 at. % C, and 1.2 at. % of N, as revealed by XPS. Both

the titanium and chlorine were below the detection limit of the XPS (< 0.1 at. %). The TiN film was etched at 460°C by 600 CVE 'cycles', where each etch cycle was comprised of 3 s long CCl_4 pulse followed by 6 s long N_2 purge. After 600 etch cycles, about 30 nm TiN film was anticipated to have been etched. Keeping real etch applications in mind, this over-etch condition was deliberately chosen to remove any TiN remnants from the SiO_2 surface. Moreover, it was important to study possible surface contamination arising from the etch process itself. The XPS analysis in figure 5 suggests that the surface is mostly composed of silicon, oxygen and some adventitious carbon. In addition, about 1.2 at.% nitrogen is seen. Titanium and chlorine were not detected. The detection limit of the particular XPS used here is 0.1 at.%. The nitrogen and carbon signals were detected around 399.1 eV (± 0.1 eV) and 284.8 eV (± 0.2 eV), respectively, and are most probably due to organic surface contamination. Hence they can be associated with handling, storage and transportation of samples within non clean-room environment. The unetched silicon dioxide substrate shows no damage and matches with reference thermal SiO_2 films.

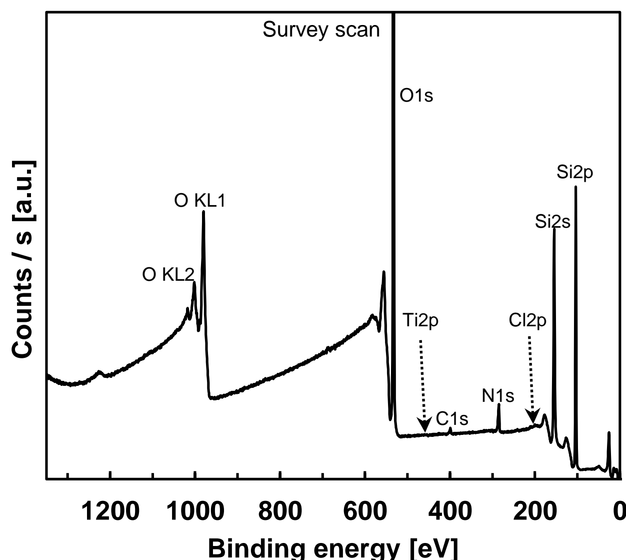

Figure 5: An X-ray photoelectron spectroscopy of SiO_2 surface after complete removal of TiN film by CCl_4 based CVE process at 460°C.

.

The same sample from the Figure 5 was subjected to a cross-sectional bright field transmission electron microscopy (BF-TEM). The BF-TEM images shown in Figure 6 reveal that TiN was

completely removed from the SiO_2 surface by the CCl_4-only etch process. Spin-on carbon was deposited prior to the TEM imaging for highlighting the material contrast. The unetched sample is shown for reference and was not exactly the same sample. The TEM image depicts that after complete removal of the TiN film from the SiO_2 surface, the surface appears to be clean and free of any surface contaminants from either the TiN film or the etch process.

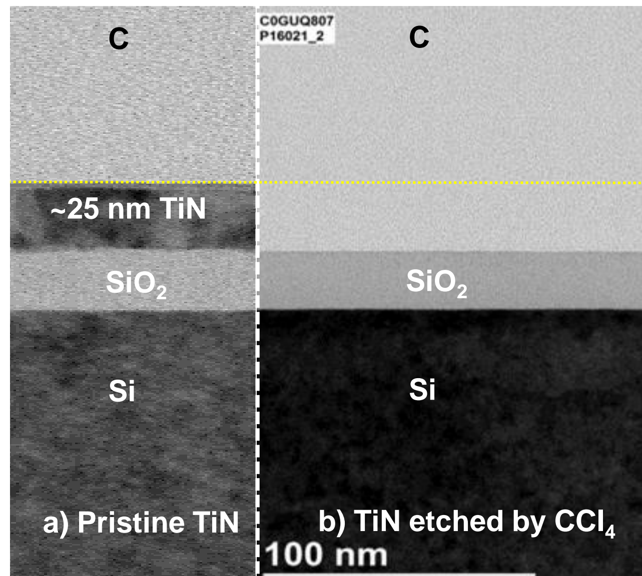

Figure 6: BF-TEM images of a) the reference unetched 25 nm TiN film on 22 nm SiO_2 film, b) after complete etching of 25 nm TiN film by 600 cycles of each 3 s long CCl_4 pulse separated by 6 s of N_2 purges.

Figure 7 plots an XPS depth profile of the elements found in an about 9 nm TiN film remaining when the etch process was incomplete. The TiN film was etched by 300 cycles of the NbF_5 - CCl_4 etch process at 460°C. The total of 60 s sputter time is estimated to etch about 1.8 nm of the TiN film. From the figure it can be seen that the surface contains about 26 at.% carbon, 31 at.% oxygen, 20 at.% nitrogen, 15 at.% titanium and about 5 at.% niobium. In addition, small amounts of silicon and fluorine were also detected with both being below 2 at.%. The silicon signal is from the SiO_2 film underneath the TiN film. After 15 s of argon ion sputtering, the carbon signal is dropped to about 4 at.% and goes further down to 3 at.% after one minute of sputtering. The atomic percentages for titanium, nitrogen and oxygen are observed around 24, 32 and 28 respectively after sputtering the surface for 15 s. A fairly high niobium amount from 5 to

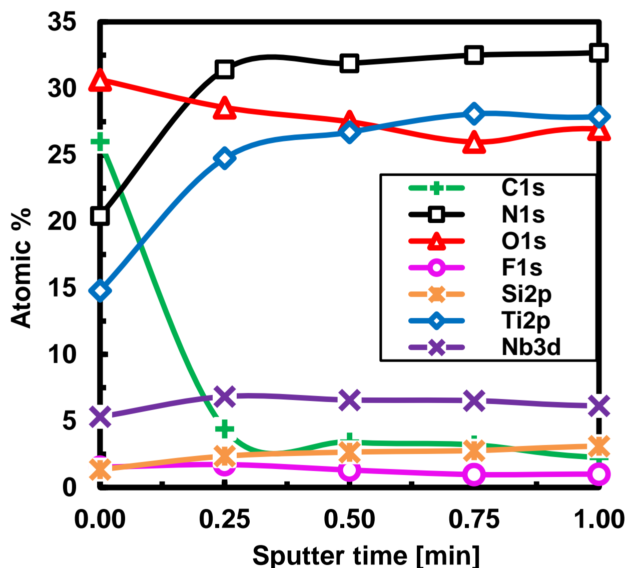

Figure 7: An XPS depth profiling through remaining TiN film after partial etching at 460°C. Total 300 cycles were performed with 0.5 s of both NbF_5 and CCl_4 pulse lengths with 6 s of N_2 purges

6 at.% along with fluorine of about 0.9-1.7 at.% may indicate that the NbF_5 is capable of either reacting or dissociating on TiN or the TiN surface modified by CCl_4. The presence of niobium is evidently consistent with the DFT adsorption studies discussed in section S1 of the SI. After sputtering for a minute, the presence of significant amounts of niobium, fluorine and carbon inside the top layer of the TiN films may be attributed to various reasons such as surface diffusion of the elements at etch temperatures preferentially through TiN grain boundaries, or increased surface area due to preferential etching along grain boundaries. They can also result from energetic argon ions bombarding the atoms deeper into the film. The absence of chlorine on or in the post-etch TiN layer points towards the formation of volatile products containing chlorine such as $TiCl_3$, $TiCl_4$, $NbFCl_3$, $NbClF_4$, and ClCN. All these compounds are predicted by the DFT simulation results.

Figure 8 is a series of TEM images taken from 3-D horizontal FIN structures. For a reference, schematic 1 provides an idea of such a 3-D structure where the blue horizontal fins are SiO_2 fins and the black back-bone is silicon. This 3-D structure was coated by a thin ALD TiN film[35] with extremely high conformality. One big advantage of gas-phase chemical etching over plasma-based etching is its capability to etch material from non line-of-sight features of this sort. Another advantage can be maintaining conformality during the etching or thinning of the films. However,

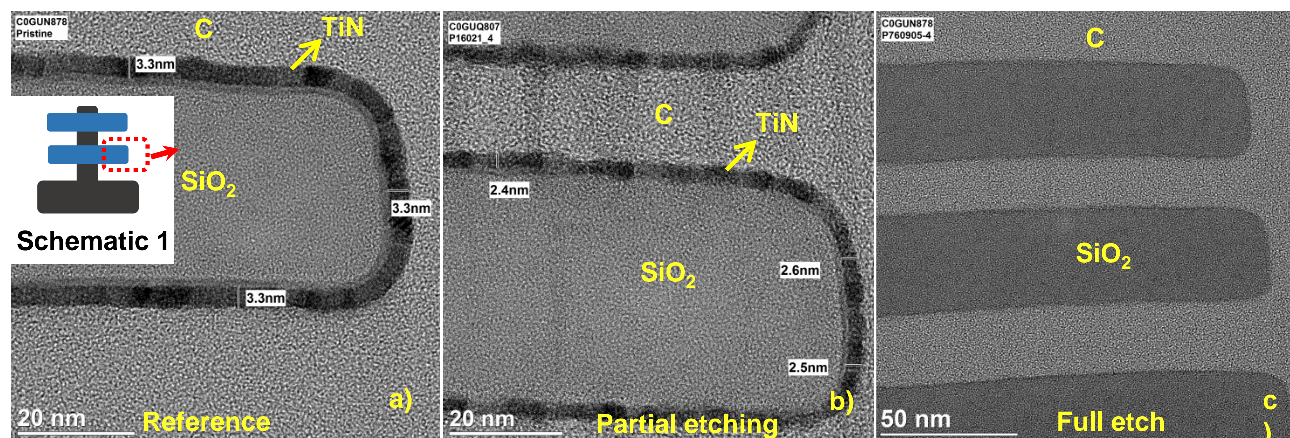

Figure 8: Cross-sectional bright field transmission electron micrograph (BF-TEM) of 3D structures: a) about 3.3 nm TiN film deposited on SiO_2 fins with lateral cavities, b) the same after about 0.8 nm TiN is etched by the NbF_5 - CCl_4 etch-process, and c) after removing the TiN film completely. The etching was performed at 460°C.

the non self-limiting gas-phase chemical etching reactions can also affect the conformality. In order to improve the etch conformality, another etchant or control-reactant can be introduced to either improve conformality or modify the etch rate such that etching from non-line-of-sight features may follow more uniform removal.

In Figure 8 a), a reference SiO_2 fin structure is covered by on average 3.3 nm pristine TiN film. The goal of this etching test was to observe the etch conformality and isotropic nature of the binary NbF_5 - CCl_4 etch process. The same sample was subjected to the binary etch process and from Figure 8 b) it can be concluded that after removal of about 0.8 nm of TiN conformally, no significant increase in the surface defects is observed. After applying over-etch the TiN is removed completely as seen in Figure 8 c). From these TEM images, no etching of SiO_2 fins was observed, thus confirming the selectivity.

Summary

We successfully demonstrated two novel gas-phase etching processes for titanium nitride. The binary etching process is based on alternate exposures of NbF_5 - CCl_4, each separated by N_2 purge. The chemical vapor etch (CVE) etch process utilizes CCl_4 exposures alone in a pulsed

fashion. In addition, the selective etching of TiN with respect to SiO_2, Si_3N_4, and Al_2O_3 was also demonstrated. Furthermore, the gas-phase etching reported here also exhibits non-directional etching from non-line-of-sight features.

From the first principles based DFT thermochemistry simulations the possible reactions and the candidate products involved in TiN etching were assessed. The surface etch mechanism is also presented in the SI section.

In a two-step etch process, the DFT MD studies predict that the NbF_5 is able to fluorinate the TiN surface but is unable to etch it by itself. This non-etching is attributed to the formation $NbNF_x$ species that are difficult to desorb from the surface. In corroboration with this, the presence of Nb and F on surface was confirmed by XPS in figure 7.

However, the simulations predict that in NbF_5 - CCl_4 etch process, NbF_5 could enhance the etch rate (favorable reaction free energy compared to CCl_4 only process) and this was experimentally verified. The Ti-F bonds are stronger and highly polar when compared to Ti-Cl bonds.[51] Thus, in comparison to Cl covered TiN surfaces, F covered TiN surfaces are more favorable for etching.

In the etching step, the CCl_4 has a tendency to chlorinate the Ti-F bonds and Nb atoms on the surface via halide-exchange mechanism[52] and hence fluorinated TiN and surface Nb as well as N atoms are etched by CCl_4 in the form of volatile compounds such as TiF_4, $NbFCl_3$, ClCN, and $TiCl_4$.

For the NbF_5 - CCl_4 etch process, the EPC varied from 0.03 Å at 370°C to a higher value of 0.55 Å at 460°C. It was found that the EPC at 460°C increases with an increase in either NbF_5 or CCl_4 pulse durations and a no clear self-limiting behaviour is observed for either of the pulse durations.

Consistent with the simulation results, experiments found that CCl_4 is able to etch TiN spontaneously in a CVE fashion. The formation of volatile species such as $TiCl_3$ and ClCN is predicted by the thermochemical studies. The CCl_4-only CVE process shows an EPC of about 0.07 Å/cycle at 370°C, linearly increasing to about 0.3 Å/cycle at 460°C. At 460°C, for a given pulse duration, the TiN removal proceeds in a linear fashion with etch exposures.

After a complete removal of titanium nitride film by CCl_4, the XPS as well as TEM analysis revealed a SiO_2 surface with no significant amounts of residues arising either from the etch process or the TiN film itself. In case of incomplete removal of TiN by the NbF_5 - CCl_4 process, XPS showed the presence of niobium and fluorine on the remaining TiN film. The absence of chlorine on the surface suggests effective formation of volatile species containing chlorine, as predicted by the simulations. The TEM images verify uniform, conformal thinning, leading eventually to complete removal of TiN from 3D structures.

Conflicts of interest

There are no conflicts to declare.

Acknowledgements

We thank Eurofins EAG Materials Science, LLC (California, USA) for the TEM analysis. Author SKN thanks ICHEC and the Science Foundation Ireland funded computing center of Tyndall National Institute for computer time. Author SKN thanks Rita Mullins for help with reaction free energy calculations.

Supporting Information Available

The attached supplementary information includes the details on DFT calculations. In the SI, the fluorination and chlorination pulses are considered separately, reflecting true nature of alternate exposures. Moreover, the adsorption of chlorine and fluorine on TiN surface is considered.

References

(1) Busnaina, A. *Nanomanufacturing Handbook*, 1st ed.; CRC Press/Taylor & Francis, 2007.

(2) Meena, J.; Sze, S.; Chand, U.; Tseng, T.-Y. Overview of emerging nonvolatile memory technologies. *Nanoscale Research Letters* **2014**, *9*, 526–.

(3) Ritala, M.; Niinistö, J. Industrial Applications of Atomic Layer Deposition. *ECS Transactions* **2019**, *25*, 641–652.

(4) Carver, C. T.; Plombon, J. J.; Romero, P. E.; Suri, S.; Tronic, T. A.; Turkot, R. B. Atomic Layer Etching: An Industry Perspective. *Solid State Science and Technology* **2015**, *4*, N5005–N5009.

(5) Oehrlein, G.; Metzler, D.; Li, C. Atomic Layer Etching at the Tipping Point: An Overview. *ECS Journal of Solid State Science and Technology* **2015**, *4*, N5041–N5053.

(6) Kanarik, K. J.; Lill, T.; Hudson, E. A.; Sriraman, S.; Tan, S.; Marks, J.; Vahedi, V.; Gottscho, R. A. Overview of atomic layer etching in the semiconductor industry. *Journal of Vacuum Science & Technology A* **2015**, *33*, 020802.

(7) Marin, E.; Lanzutti, A.; Andreatta, F.; Lekka, M.; Guzman, L.; Fedrizzi, L. Atomic layer deposition: state-of-the-art and research/industrial perspectives. *Corrosion Reviews* **2011**, *29*, 191–208.

(8) Miikkulainen, V.; Leskelä, M.; Ritala, M.; Puurunen, R. L. Crystallinity of inorganic films grown by atomic layer deposition: Overview and general trends. *Journal of Applied Physics* **2013**, *113*, 021301–.

(9) Oviroh, P. O.; Akbarzadeh, R.; Pan, D.; Coetzee, R. A. M.; Jen, T.-C. New development of atomic layer deposition: processes, methods and applications. *Science and Technology of Advanced Materials* **2019**, *20*, 465–496.

(10) George, S. M. Mechanisms of Thermal Atomic Layer Etching. *Accounts of Chemical Research* **2020**,

(11) Fang, C.; Cao, Y.; Wu, D.; Li, A. Thermal atomic layer etching: Mechanism, materials and prospects. *Progress in Natural Science* **2018**, *28*, 667–675.

(12) Lee, Y.; George, S. M. Atomic Layer Etching of Al_2O_3 Using Sequential, Self-Limiting Thermal Reactions with $Sn(acac)_2$ and Hydrogen Fluoride. *ACS Nano* **2015**, *9*, 2061–2070, PMID: 25604976.

(13) Dadgour, H.; Endo, K.; De, V.; Banerjee, K. Grain-Orientation Induced Work Function Variation in Nanoscale Metal-Gate Transistors—Part I: Modeling, Analysis, and Experimental Validation. *IEEE Transactions on Electron Devices* **2010**, *57*, 2504–2514.

(14) Lü, L., Wei-Feng; Dai Impact of work-function variation on analog figures-of-merits for high-k/metal-gate junctionless FinFET and gate-all-around nanowire MOSFET. *Microelectronics Journal* **2019**, *84*, 54–58.

(15) Matsuura, K.; Hamada, M.; Hamada, T.; Tanigawa, H.; Sakamoto, T.; Hori, A.; Muneta, I.; Kawanago, T.; Kakushima, K.; Tsutsui, K.; Ogura, A.; Wakabayashi, H. Normally-off sputtered-MoS2 nMISFETs with TiN top-gate electrode all defined by optical lithography for chip-level integration. *Japanese Journal of Applied Physics* **2020**, *59*, 080906.

(16) Kim, H. Atomic layer deposition of metal and nitride thin films: Current research efforts and applications for semiconductor device processing. *Journal of Vacuum Science & Technology B Microelectronics and Nanometer Structures* **2003**, *21*, 2231–.

(17) Darnon, M.; Chevolleau, T.; Eon, D.; Vallier, L.; Torres, J.; Joubert, O. Etching characteristics of TiN used as hard mask in dielectric etch process. *Journal of Vacuum Science & Technology B: Microelectronics and Nanometer Structures Processing, Measurement, and Phenomena* **2006**, *24*, 2262–2270.

(18) Abraham, S. C. Performance of different etch chemistries on titanium nitride antireflective coating layers and related selectivity and microloading improvements for submicron geome-

tries obtained with a high-density metal etcher. *Journal of Vacuum Science & Technology A Vacuum Surfaces and Films* **1997**, *15*, 702–706.

(19) DeVries, S.; De Silva, E. A.; Canaperi, D.; Simon, A.; de la Pena, A. A.; Wang, W.; Maniscalco, J.; Meli, L.; Mendoza, B. Comparing PVD Titanium Nitride Film Properties and their Effect on Beyond 7 nm EUV Patterning. 31st Annual SEMI Advanced Semiconductor Manufacturing Conference (ASMC). 2020; pp 1–5.

(20) Shinde, S. L.; Ishii, S.; Nagao, T. Sub-bandgap photodetection from Titanium Nitride/Germanium heterostructure. *ACS Applied Materials & Interfaces* **2019**, acsami.9b01372–.

(21) Gosciniak, J.; Atar, F. B.; Corbett, B.; Rasras, M. CMOS-Compatible Titanium Nitride for On-Chip Plasmonic Schottky Photodetectors. *ACS Omega* **2019**,

(22) Mehmood, F.; Pachter, R.; Murphy, N. R.; Johnson, W. E. Electronic and optical properties of titanium nitride bulk and surfaces from first principles calculations. *Journal of Applied Physics* **2015**, *118*, 195302–.

(23) Patsalas, P.; Kalfagiannis, N.; Kassavetis, S. Optical Properties and Plasmonic Performance of Titanium Nitride. *Materials* **2015**, *8*, 3128–3154.

(24) Cooper, E. I.; Rajaram, R.; Payne, M.; Lippy, S. Selective High-Throughput TiN Etching Methods. *Solid State Phenomena* **2012**, *195*, 143–145.

(25) Liu, Y.; Kamei, T.; Endo, K.; O'uchi, S.; Tsukada, J.; Yamauchi, H.; Hayashida, T.; Ishikawa, Y.; Matsukawa, T.; Sakamoto, K.; Ogura, A.; Masahara, M. Nanoscale Wet Etching of Physical-Vapor-Deposited Titanium Nitride and Its Application to Sub-30-nm-Gate-Length Fin-Type Double-Gate Metal–Oxide–Semiconductor Field-Effect Transistor Fabrication. *Japanese Journal of Applied Physics* **2010**, *49*, 06GH18.

(26) Bhattacharyya, D.; Kuchibhatla, S.; Sehgal, A.; Shen, Y. P.; Haiting, W.; Prasad, J. Selective isotropic wet etching of TiN and TaN for high-k metal gate structure. *26th Annual SEMI Advanced Semiconductor Manufacturing Conference (ASMC) - Saratoga Springs, NY, USA* **2015**, 305–308.

(27) Tonotani, J.; Iwamoto, T.; Sato, F.; Hattori, K.; Ohmi, S.; Iwai, H. Dry etching characteristics of TiN film using Ar/CHF_3, Ar/Cl_2, and Ar/BCl_3 gas chemistries in an inductively coupled plasma. *Journal of Vacuum Science & Technology B: Microelectronics and Nanometer Structures Processing, Measurement, and Phenomena* **2003**, *21*, 2163–2168.

(28) Wang, Y.-Y.; Joo, Y.-H.; Kim, C.-I. Etching Characteristics of Titanium Nitride in Chlorine-Based Plasma. *Journal of Nanoscience and Nanotechnology* **2016**, *16*, 12933–12935.

(29) Marchack, N.; Papalia, J. M.; Engelmann, S.; Joseph, E. A. Cyclic Cl_2 /H_2 quasi-atomic layer etching approach for TiN and TaN patterning using organic masks. *Journal of Vacuum Science & Technology A Vacuum Surfaces and Films* **2017**, *35*, 1–9.

(30) Shinoda, K.; Miyoshi, N.; Kobayashi, H.; Izawa, M.; Ishikawa, K.; Hori, M. Rapid thermal-cyclic atomic-layer etching of titanium nitride in CHF3/O_2 downstream plasma. *Journal of Physics D: Applied Physics* **2019**, *52*, 475106.

(31) Lee, Y.; George, S. M. Thermal Atomic Layer Etching of Titanium Nitride Using Sequential, Self-Limiting Reactions: Oxidation to TiO_2 and Fluorination to Volatile TiF_4. *Chemistry of Materials* **2017**, *29*, 8202–8210.

(32) Sharma, V.; Blomberg, T.; Haukka, S.; Cembella, S.; Givens, M. E.; Tuominen, M.; Odedra, R.; Graff, W.; Ritala, M. Thermal gas-phase etching of titanium nitride (TiN) by thionyl chloride ($SOCl_2$). *Applied Surface Science* **2020**, *52*, 148309.

(33) Dingemans, G.; Van Helvoirt, C.; Van de Sanden, M.; Kessels, W. M. ECS Transactions [ECS 219th ECS Meeting - Montreal, QC, Canada (May 1 - May 6, 2011)] - Plasma-Assisted Atomic Layer Deposition of Low Temperature SiO_2. 2011; pp 191–204.

(34) Gosset, L.; Damlencourt, J.-F.; Renault, O.; Rouchon, D.; Holliger, P.; Ermolieff, A.; Trimaille, I.; Ganem, J.-J.; Martin, F.; Séméria, M.-N. Interface and material characterization of thin Al_2O_3 layers deposited by ALD using TMA/H_2O. *Journal of Non-Crystalline Solids* **2002**, *303*, 0–23.

(35) Ahn, C. H.; Cho, S. G.; Lee, H. J.; Park, K. H.; Jeong, S. H. Characteristics of TiN thin films grown by ALD using $TiCl_4$ and NH_3. *Metals and Materials International* **2001**, *7*, 621–625.

(36) Michael, J. V.; Lim, K. P.; Kumaran, S. S.; Kiefer, J. H. Thermal decomposition of carbon tetrachloride. *Journal of Physical Chemistry* **1993**, *97*, 1914–1919.

(37) Huang, F.; Zhao, H.; Yan, A.; Li, Z.; Liang, H.; Gao, Q.; Qiang, Y. In situ thermal decomposition for preparation of Nb_3O_7F/Nb_2O_5 hybrid nanomaterials with enhanced photocatalytic performance. *Journal of Alloys and Compounds* **2017**, *695*, 489–495.

(38) Konings, R. J. M. The composition of niobium pentafluoride vapor. *Structural Chemistry* **1994**, *5*, 9–13.

(39) Sharma, V.; Elliott, S. D.; Blomberg, T.; Haukka, S.; Givens, M. E.; Tuominen, M.; Ritala, M. Thermal Atomic Layer Etching of Aluminum Oxide (Al_2O_3) Using Sequential Exposures of Niobium Pentafluoride (NbF_5) and Carbon Tetrachloride (CCl_4): A Combined Experimental and Density Functional Theory Study of the Etch Mechanism. *Chemistry of Materials* **2021**, *33*, 2883–2893.

(40) Kresse, G.; Furthmuller, J. Efficient iterative schemes for ab initio total-energy calculations using a plane-wave basis set. *Phys. Rev. B* **1996**, *54*, 11169.

(41) Kresse, G.; Joubert, D. From ultrasoft pseudopotentials to the projector augmented-wave method. *Phys. Rev. B* **1999**, *59*, 1758.

(42) Perdew, J. P.; Burke, K.; Ernzerhof, M. Generalized gradient approximation made simple. *Phys. Rev. Lett.* **1996**, *77*, 3865–.

(43) Blochl, P. Projector augmented-wave method. *Phys. Rev. B* **1994**, *50*, 17953.

(44) TURBOMOLE V6.2 2010, a development of University of Karlsruhe and Forschungszentrum Karlsruhe GmbH, 1989-2007, TURBOMOLE GmbH, since 2007; available from `http://www.turbomole.com` last accessed 27/11/2019. 2010.

(45) Togo, A.; Tanaka, I. First principles phonon calculations in materials science. *Scr. Mater.* **2015**, *108*, 1–5.

(46) Ramanath, G.; Greene, J. E.; Carlsson, J. R. A.; Allen, L. H.; Hornback, V. C.; Allman, D. J. W deposition and titanium fluoride formation during WF_6 reduction by Ti: Reaction path and mechanisms. *Journal of Applied Physics* **1999**, *85*, 1961–1969.

(47) Sekimoto, H.; Nose, Y.; Uda, T.; Sugimura, H. Preparation and Properties of Trivalent Titanium Compounds, $TiCl_3$ and TiOCl. *High Temperature Materials and Processes* **2011**, *30*, 435–440.

(48) Kelley, K.; Mah, A. *Metallurgical Thermochemistry of Titanium*; Report of investigations / U.S. Dept. of the Interior, Bureau of Mines; University of Michigan, 1959.

(49) Pike, F. P.; Foster, C. T. Vapor Pressure and Boiling Point of Titanium Tetrachloride. *Journal of Chemical & Engineering Data* **1959**, *4*, 305–306.

(50) Hall, E. H.; Blocher, J. M.; Campbell, I. E. Vapor Pressure of Titanium Tetrafluoride. *Journal of The Electrochemical Society* **1958**, *105*, 275–278.

(51) Webb, S. P.; Gordon, M. S. Intermolecular Self-Interactions of the Titanium Tetrahalides TiX_4 (X = F, Cl, Br). *Journal of the American Chemical Society* **1999**, *121*, 2552–2560.

(52) Evano, G.; Nitelet, A.; Thilmany, P.; Dewez, D. F. Metal-Mediated Halogen Exchange in Aryl and Vinyl Halides: A Review. *Frontiers in Chemistry* **2018**, *6*, 1–18.

Supplementary Information: Combining Experimental and DFT Investigation of the Mechanism Involved in Thermal Etching of Titanium Nitride Using Alternate Exposures of NbF_5 and CCl_4, or CCl_4 only

Varun Sharma,[*,†] Suresh Kondati Natarajan,[¶] Simon D. Elliott,[§] Suvi Haukka,[†]
Marko Tuominen,[†] Tom Blomberg,[||] and Mikko Ritala[*,‡]

†*ASM Microchemistry Oy, Pietari Kalmin katu 3 F2, 00560 Helsinki, Finland*

‡*Department of Chemistry, University of Helsinki, FI-00014 Helsinki, Finland*

¶*Department of Electrical Engineering and Automation, Aalto University, Espoo 02156, Finland*

§*Schrödinger, 120 West 45th Street, New York, NY 10036-4041, USA*

||*Department of Chemistry and Materials Science, Aalto University, Espoo, Uusimaa 02150, Finland*

⊥*Currently at Picosun Oy, Masala, Finland*

E-mail: varun.sharma@asm.com,varun.sharma@helsinki.fi; mikko.ritala@helsinki.fi

S0: Computational details

In this supporting information, explicit atomistic mechanisms involved in the etching of TiN using NbF_5 and CCl_4 are provided. We have used TiN(2 1 1), a stepped surface for this study. Stepped surfaces are the most suitable for this type of analysis as they have high surface energy and they are

often more reactive than the flat surfaces. A 9.3 Å thick (2×2) supercell of the TiN (2 1 1) surface ($Ti_{96}N_{96}$) with a surface area of 1.74 nm^2 and computed surface energy of 3.8 J/m^2 is chosen for the surface model, which consists of 4 $Ti_{24}N_{24}$ layers with a rigid bottom layer. A Monkhorst-Pack K-point mesh of 2×3×1 is used during the geometry relaxation.

Binding/adsorption energies (E_{ads}) are given by

$$E_{\text{ads}} = E_{\text{int}} - \sum E_{\text{non-int}}, \tag{1}$$

in which E_{int} is the energy of the interacting system where the molecule is adsorbed on the surface of the material and $E_{\text{non-int}}$ are the energies of the participating but non-interacting systems such as the energy of the molecule in gas phase and energy of the bare surface.

S1: Fluorination pulse

In this section we present the results of first principles based adsorption simulations where NbF_5 molecules are reacting with the TiN(2 1 1) surface. Homolytic dissociation of NbF_5 in gas phase is very endoergic requiring 7.3 eV to remove one F ligand and 9.9 eV to remove F_2. Thus, the TiN surface shown in Figure S1 has to satisfy this energy requirement and catalyse the NbF_5 dissociation. The step edge present in the TiN(2 1 1) surface is especially a favourable reactant binding spot.

In the minimum energy geometry of isolated NbF_5 molecule, three F ligands are bound along the equatorial plane of the molecule each with an Nb-F bond length of 1.85 Å and two F ligands are found in either sides of the polar axis of the molecule with an Nb-F bond length of 1.88 Å. Since the polar Nb-F bond length is longer, we adsorbed the molecule with a polar F ligand close to a Ti atom along the step edge of the surface. On adsorption, the NbF_5 molecule does not dissociate at 0 K, as shown in Figure S2, due to the presence of kinetic barriers for the Nb-F bond dissociation. However, the NbF_5 binding energy to the surface is about -0.9 eV and we see an extended bond length of Nb-F close to the surface (from 1.88 Å to 2.05 Å) which indicates that this bond will

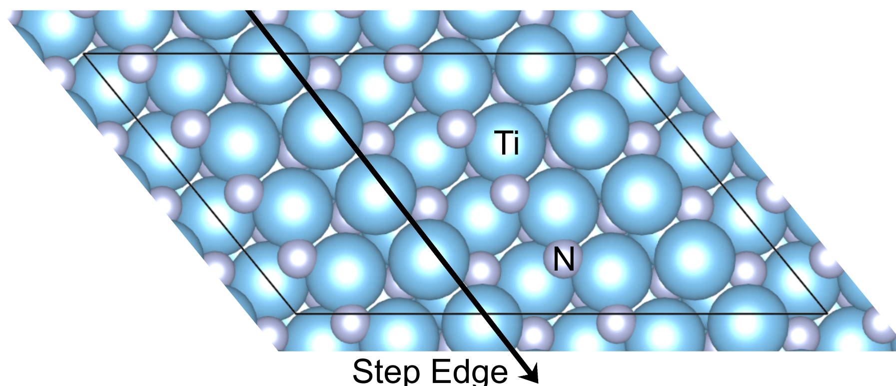

Figure S1: Bare surface of TiN(2 1 1) with step edge marked by an arrow. Grey atoms are Ti and blue atoms are N.

break easily at elevated temperatures. The distance of the newly formed Ti-F bond on the surface is 2.05 Å.

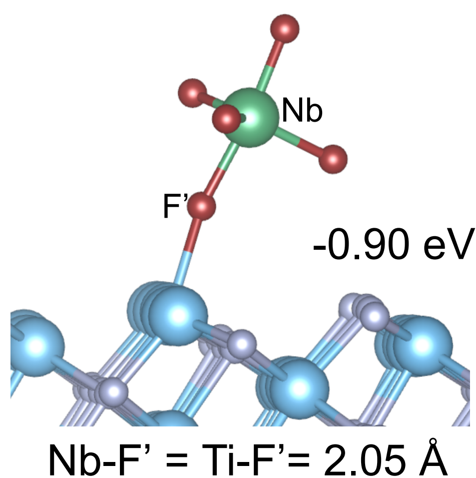

Figure S2: Intact adsorption of NbF_5 molecule on TiN(2 1 1) surface. The red and green are niobium and fluorine atoms, respectively.

We performed a 5 ps MD simulation at 400 K at DFT level starting from the above local minimum geometry. Within 1.7 ps, 4 Nb-F bonds are dissociated consecutively from the NbF_5 molecule and the F atoms adsorb at the TiN surface. This very rapid dissociation suggests that barriers to the dissociation of NbF_5 can be overcome easily on the modelled TiN(2 1 1) surface at 400 K. We extracted a few geometries from the simulation and relaxed them to find unique minimum energy geometries as shown in Figure S3.

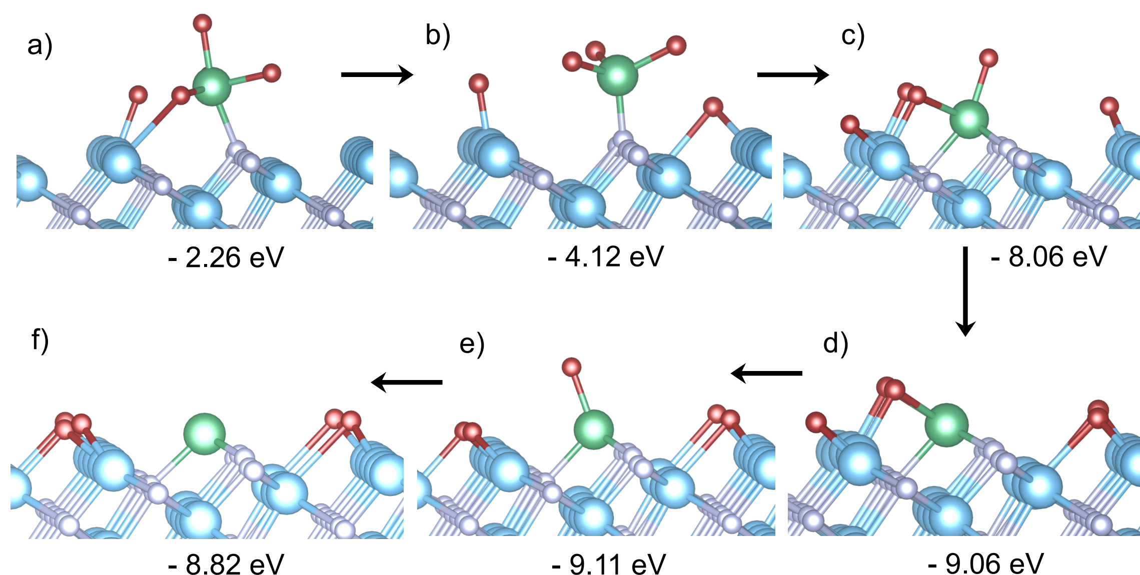

Figure S3: Minimum energy geometries of NbF_5 adsorbed on TiN(2 1 1) surface (at 0 K) which are extracted from an MD simulation at 400 K.

In the minimum energy geometries shown in Figure S3a-e we find a continuous decrease in the binding energy, from -0.90 eV up to -9.11 eV, as more Nb-F bonds get dissociated and Ti-F formed. The most favourable geometry is Figure S3e where the Nb is bound to the surface, coordinating with three surface N atoms, and it is left with one F ligand pointing away from the surface. This suggests that NbF_5, at 400 K, dissociates readily on the TiN(2 1 1) surface and the surface will be covered by Nb-N and Ti-F terminations at the end of this pulse. Although not observed in the MD trajectory, we also studied full dissociation of NbF_5 molecule as shown in Figure S3f, however, this configuration was less favourable than the one in Figure S3e. In Figure S4, we have shown a NbF_5 saturated TiN surface model where the Nb atoms are trapped next to the step edge coordinated to surface N atoms while the F atoms are found atop the Nb atoms, at the 3 fold Ti sites and at the bridge sites connecting Ti and Nb atoms along the step edges. This geometry corresponds to a NbF_5 coverage of 2.3 molecules/nm^2, a dissociated F coverage of 9.0 F/nm^2 and a net binding energy of -7.3 eV/NbF_5. The Nb and F that have this way been deposited on the surface will block further reaction with NbF_5, which must result in self-limiting reaction.

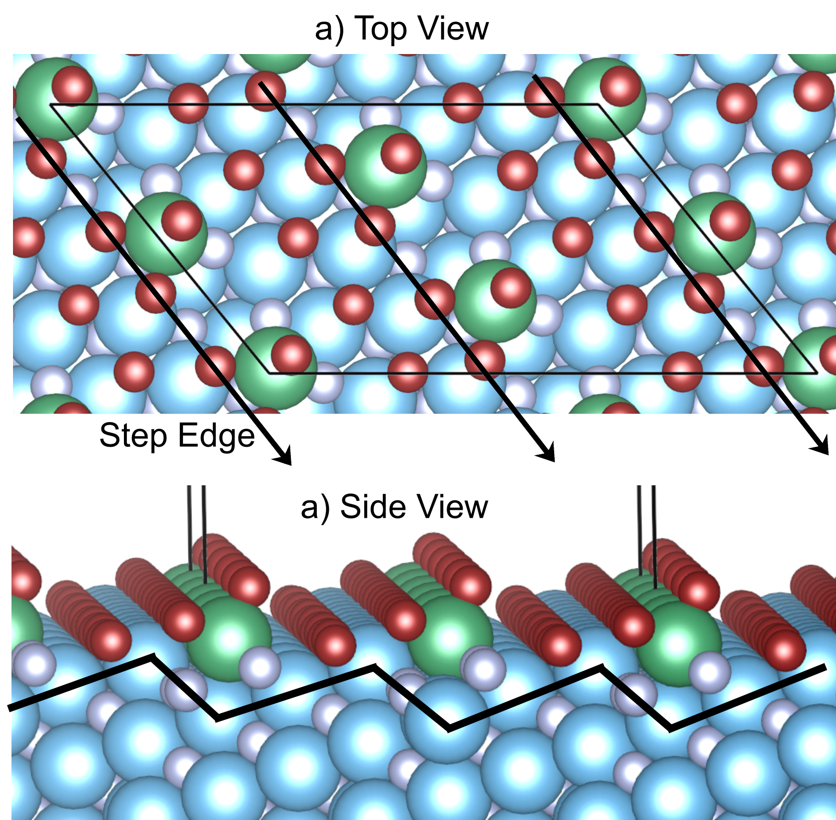

Figure S4: A minimum energy geometry showing a NbF_5 saturated surface of TiN(2 1 1). The Nb atoms can be seen trapped near the step edge. panels a) and b) show the top and side views, respectively. The green and red are niobium and fluorine atoms, respectively.

S2: Chlorination pulse

We will use the above surface geometry for the CCl_4 adsorption in the next pulse. Before we look into those results we would like to validate our thermochemical prediction for the CCl_4 pulse (R9 in Table 2 of main text). From explicit surface adsorption calculations, we find that the CCl_4 molecule spontaneously dissociates on the bare TiN at 0 K, donates a Cl ligand to the surface, and drifts off in to the vacuum as CCl_3 fragment. This in contrast to the NbF_5 adsorption, which did not dissociate spontaneously. This is proof that CCl_4 reacts strongly with the bare TiN surface when compared to NbF_5. We also performed a short 3 ps long MD simulation at DFT level of CCl_4 adsorbed on the bare TiN surface which resulted in a complete dissociation of CCl_4 molecule within just 0.74 ps and formation of three surface Ti-Cl and a surface bound CNCl, which is the proposed by-product of this reaction.

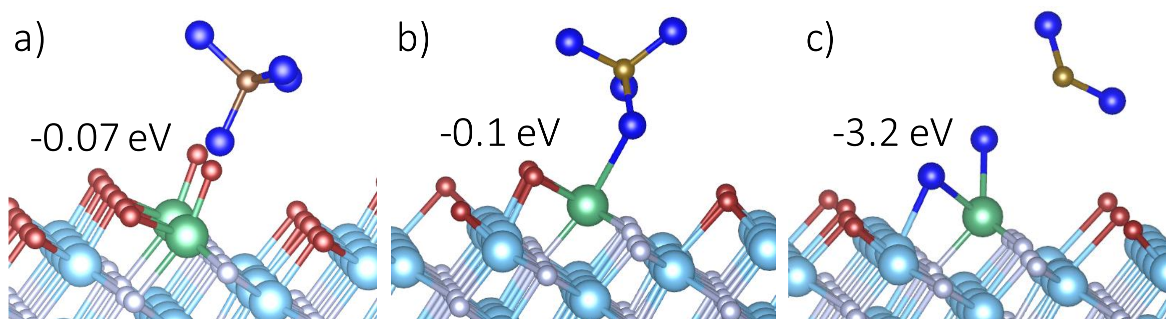

Figure S5: A minimum energy geometry of intact CCl_4 adsorbed at the Nb_XF_Y covered TiN surface at 0 K.

A CCl_4 molecule did not bind strongly to the fluorine covered TiN surface at 0 K due to net repulsion between the Cl atoms and surface bound F ligands. The most favourable geometry found in our investigation with a binding energy of -0.07 eV is given in Figure S5a. In this configuration, one of the Cl atoms of CCl_4 is directed at the surface towards the Nb atoms. In all the other configurations where the C-Cl bond is directed towards the surface Ti/F atoms, the CCl_4 molecule did not physisorb on the surface but was pushed back into the vacuum. This suggests that Nb sites are important for CCl_4 to react with when the rest of the surface is covered with F. On the other hand, if the coverage of NbF_5 is sparse, then the CCl_4 molecule will readily dissociate on the Ti

rich surface region.

Since we have already established that CCl_4 spontaneously dissociated on the bare TiN surface, we now discuss the CCl_4 interaction with F-free Nb sites. We adsorbed a CCl_4 molecule close to the Nb atom in the geometries shown in Figures S3d and S3e and the resulting relaxed geometries are shown in Figures S5b and S5c, respectively. We find that a favourable binding (-0.1 eV) between the Cl atoms and Nb atom is possible (Figures S5b) even when the Nb atom is weakly bound to 2 F atoms, when they are simultaneously bound also to surface Ti atoms. A strong dissociative adsorption of CCl_4 (-3.2 eV) is possible when the Nb atom is free of Nb-F bonds (Figures S5b). Based on the above computational results, we propose that the ALE of TiN proceeds by self-limiting dissociative adsorption of NbF_5 in the first pulse followed by the dissociative adsorption of CCl_4 catalysed by the Nb sites in the second pulse leading to the etch of TiN.

We do not look at the mechanism of formation and desorption of all the possible volatile species in this paper as there are very many product combinations involved and computing all reaction pathways is not in the scope of this paper.

S3: Adsorption of Cl and F onto TiN

Figure S6, reveals that on TiN surface F adsorbs more strongly than Cl at various surface coverages and this difference in binding is more pronounced at higher coverages. Although both F and Cl are halogens, F being in the second period in the periodic table as compared to Cl in the third period would naturally result in stronger binding due to small atomic radius and increased electronegativity of F. What this means is that, when F adsorbs on the TiN surface, the strong and highly polar Ti-F bonds[1] are formed on the surface. These strong surface bonds will in turn weaken the bonding of the surface Ti atoms with the sub-surface atoms, this effect is needed for the removal of the surface Ti atoms. Thus, in comparison to Cl covered TiN surface, F covered TiN surface will be favorable for etching. This could be the reason for the catalytic behavior of NbF_5, especially due to its dissociation on TiN surface.

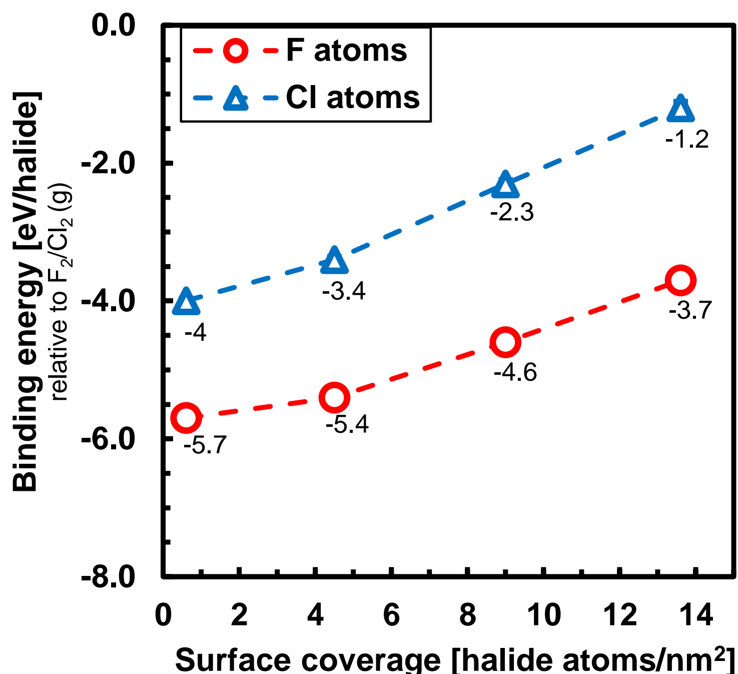

Figure S6: Binding energy of chlorine and fluorine atoms on TiN surface at varying halide atoms surface coverage at 0 K.

S4: Change in the Gibbs free energy with temperature

Figure S7 shows a change in the Gibbs free energy at various temperatures for considered reactions R1 to R9 (see Tables 1 and 2 in the main article). From the figure it is clear that only reactions R3, R4, R5 and R9 are feasible atleast upto the experimented etch temperature i.e. 460°C. From these reactions, the volatile titanium-containing etch products are predicted to be $TiCl_3$, $TiCl_4$, and TiF_4.

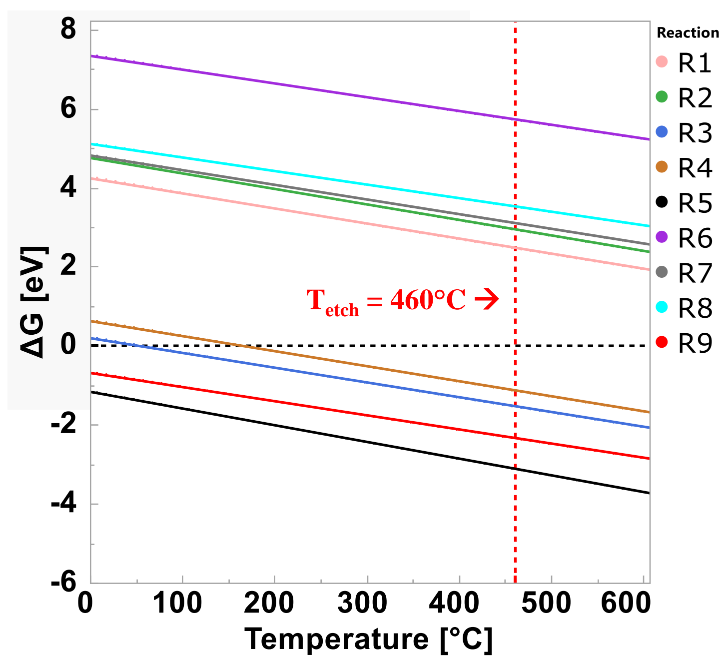

Figure S7: A change in the Gibbs free energy is plotted at various temperatures.

References

(1) Webb, S. P.; Gordon, M. S. Intermolecular Self-Interactions of the Titanium Tetrahalides TiX_4 (X = F, Cl, Br). *Journal of the American Chemical Society* **1999**, *121*, 2552–2560.